Stellar properties indicating the presence of hyperons in neutron stars

Andreas Bauswein [1,2] Aristeidis Nikolaidis [1,3] Georgios Lioutas [4] Hristijan Kochankovski,[5] Prasanta Char [6,7] Chiranjib Mondal [8] Micaela Oertel [9,10] Laura Tolos [11,12] Nicolas Chamel [8] and Stephane Goriely [8]

[1] *GSI Helmholtzzentrum für Schwerionenforschung, Planckstraße 1, D-64291 Darmstadt, Germany*

[2] *Helmholtz Forschungsakademie Hessen für FAIR (HFHF), GSI Helmholtzzentrum für Schwerionenforschung, Planckstraße 1, D-64291 Darmstadt, Germany*

[3] *Department of Physics and Astronomy, Ruprecht-Karls-Universität Heidelberg, Im Neuenheimer Feld 226, 69120 Heidelberg, Germany*

[4] *Heidelberger Institut für Theoretische Studien (HITS), Schloss-Wolfsbrunnenweg 35, 69118 Heidelberg, Germany*

[5] *Departament de Física Quàntica i Astrofísica and Institut de Ciències del Cosmos, Universitat de Barcelona, Martí i Franquès 1, 08028 Barcelona, Spain*

[6] *Departamento de Física Fundamental and IUFFyM, Universidad de Salamanca, Plaza de la Merced S/N, E-37008 Salamanca, Spain*

[7] *Space Sciences, Technologies and Astrophysics Research (STAR) Institute, Université de Liège, Bât. B5a, 4000 Liège, Belgium*

[8] *Institut d'Astronomie et d'Astrophysique, CP-226, Université Libre de Bruxelles, 1050 Brussels, Belgium*

[9] *Observatoire Astronomique de Strasbourg, CNRS, Université de Strasbourg, 11 rue de l'Université, 67000 Strasbourg, France*

[10] *LUX, CNRS, Observatoire de Paris, Université PSL, Université Paris Cité, 5 place Jules Janssen, 92195 Meudon, France*

[11] *Institute of Space Sciences (ICE, CSIC), Campus UAB, Carrer de Can Magrans, 08193 Barcelona, Spain*

[12] *Institut d'Estudis Espacials de Catalunya (IEEC), 08860 Castelldefels, Barcelona, Spain*

(Received 14 July 2025; accepted 26 January 2026; published 6 March 2026)

We describe distinctive stellar features indicating the presence of hyperons in neutron stars as compared to purely nucleonic systems. A strongly negative curvature of the mass-radius relation $R(M)$ is characteristic of hyperons, which can be determined from measurements of neutron stars with three different masses. Similarly, a reduced second derivative of the tidal deformability as a function of mass $\lambda(M)$ points to hyperonic degrees of freedom in neutron star matter. The slopes of such curves $R(M)$ and $\lambda(M)$ can distinguish a hyperonic equation of state from purely nucleonic models if they appear increased [decreased for $\lambda(M)$] relative to the maximum mass of neutron stars.

DOI: 10.1103/ygtr-ktqk

I. INTRODUCTION

Non-nucleonic degrees of freedom such as hyperons are widely discussed as possible components of neutron star (NS) matter. Since the constituents of high-density matter and their interactions are not precisely known, the equation of state (EoS) of NSs is subject to uncertainties [1–7]. The EoS of cold NSs in beta equilibrium is a unique relation between pressure and energy density that unambiguously determines the stellar structure like the mass-radius relation or the tidal deformability of stars in binaries through the relativistic stellar structure equations [8–12]. By measuring stellar parameters of NSs, it is thus possible to probe the EoS and learn about the fundamental building blocks of high-density matter, e.g., the presence of hyperons. These efforts are linked to numerous theoretical and experimental studies to understand the interactions between hyperons and nucleons [13–15].

Many theoretical models of the EoS with different degrees of sophistication have been devised for purely nucleonic matter as well as for matter with hyperons [16]. The occurrence of hyperons is known to be associated with a softening of the EoS, which would generally result in a reduction of NS radii and the maximum mass of NSs [6,17–23]. However, to the best of our knowledge, there is to date no clear and distinctive *quantitative* measure known based on which a discrimination between purely nucleonic and hyperon-admixed matter in NSs is possible employing measurements of stellar structure properties. Only a statistical approach considering the slope of the mass-radius relation has been discussed in Ref. [24], where radii decreasing with mass in the range 1.2 to 1.4 $M_\odot$ point to a lower likelihood of hyperons being present in NSs. Statistical arguments have also been employed in Ref. [25], and cooling observations may also provide valuable information on the composition of NSs [18,26–36].

The capabilities of NS observations to determine stellar properties are continuously growing, for instance, with the x-ray timing measurements of Neutron star Interior Composition Explorer (NICER) [37–40] or with gravitational-wave observatories [41–44], and several new instruments are projected to advance these efforts in the next decade [45–48]. However, the current lack of a distinct feature of hyperons imprinted on the stellar structure parameters implies that even precise measurements of NS properties would not allow to infer the hyperon content of NSs and solve the "hyperon puzzle" (cf. Refs. [6,14,15,17–23,49,50]).

In this paper, we propose to consider the curvature and the second derivative with respect to mass of the mass-radius curve and the mass-tidal deformability relation to identify the presence of hyperons in NSs or, generally, non-nucleonic degrees of freedom. Those parameters quantify the bending toward smaller NS radii with increasing mass and are found to be characteristically lowered if hyperons are present. We also find that the slope of the aforementioned relations at a fixed mass compared to the maximum mass of NSs can indicate hyperonic degrees of freedom. Observationally, these characteristics are accessible by considering several measurements of NSs with different masses. The stellar structure does not give a handle on which mechanisms and degrees of freedom are responsible for softening the EoS. Thus, ultimately, the properties discussed here can only indicate that non-nucleonic degrees of freedom soften the EoS so strongly that it is incompatible with purely nucleonic models. Non-nucleonic degrees of freedom appearing via a first-order phase transition (such as quarks in many models) result in a characteristic kink in the mass-radius relation, which has been discussed as potential signature for many years [1,2,6,51], and thus identifying a quantitative signature for a smoother occurrence of non-nucleonic degrees of freedom remains a major challenge.

II. EOS SAMPLE

We base our study on a very large set of microphysical EoS models for matter in beta equilibrium and at zero temperature. This sample includes 47 hyperonic models and 248 purely nucleonic EoSs (see the Appendix). These tables stem from three sources, to which we refer for more details. One subset consists of various models that we previously used in NS merger simulations [52,53] and which were obtained through private communication or various webpages [54–91]. Another larger set of models is taken from the Compose repository [16], where we include all baryonic NS matter models with a maximum mass of at least 1.9 $M_\odot$ [5,70,92–153]. We supplement our sample with a selection of models for purely nucleonic [145,154] and hyperonic [155,156] matter constructed from covariant density functional theory. Overall, our sample represents a large variety of models, which are based on different theoretical frameworks (e.g., nonrelativistic and relativistic density functional methods) and adjusted to different experimental data (properties of nuclear matter and nuclei). We include parametric models only if they are fitted to reproduce actual microphysical models and we refrain from using agnostic approaches to the EoS since they do not inform about the composition and thus the potential presence of hyperons. All EoS models reach a maximum NS mass of at least 1.9 $M_\odot$, which is somewhat below the limit imposed by heavy pulsars [157–161], but it is advantageous to slightly enlarge the range of possible models (only nine hyperonic and eight purely nucleonic models have $M_{\rm max} < 2.0\ M_\odot$). Otherwise, we do not employ any additional selection criteria for the EoS sample albeit various constraints might have already been imposed during the development of certain EoS models.

Since our sample includes many of the currently available microphysical EoS models, we assume that our set is representative and covers sufficiently well the span of possible microphysical EoSs of purely nucleonic matter. The number of EoSs with hyperons is smaller because of the limited availability of such models, although the sample still covers a broad range with regard to the resulting stellar properties and, for instance, the EoSs from Ref. [155] have been chosen to represent the possible variations within the respective model. For our line of reasoning, it suffices to show that hyperonic models exist that behave different from all possible purely nucleonic EoSs.

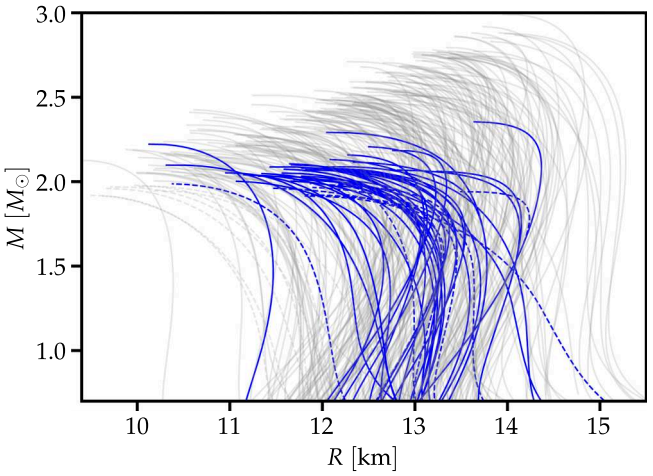

FIG. 1. Mass-radius relations of NSs considered in this study for hyperonic EoSs (blue) and purely nucleonic EoSs (gray). Dashed curves indicate EoSs with $M_{\rm max} < 2.0\ M_\odot$.

III. RADIUS CURVES

For all EoSs, we compute the circumferential radii R and tidal deformability λ as a function of gravitational mass M using the extended set of relativistic stellar structure equations [8–12]. λ is given by $\frac{2}{3}k_2R^5$ with the tidal Love number k_2. All curves are provided in the Appendix. In mass-radius relations (Fig. 1), hyperonic models often exhibit the tendency to more strongly bend over to smaller radii with increasing mass. We intend to assess and quantify this effect as a characteristic indicator of hyperons in NSs.

To this end, we propose to consider the curvature of the curves $R(M)$. We compute $\kappa_R = \frac{d^2R}{dM^2}(1+(\frac{dR}{dM})^2)^{-3/2}$, where we obtain the first and second derivatives by finite differencing of the $R(M)$ curves [162]. Geometrically κ quantifies the inverse of the curvature radius of a curve. Using $G = c = 1$, we express radii (and λ) in units of mass such that derivatives and κ are dimensionless.

Figure 2 shows κ_R as a function of mass for hyperonic and purely nucleonic EoS models. As may already be obvious from the mass-radius relations, the curvature typically decreases with mass turning from positive to negative κ_R and reaches a minimum to finally rise as M goes to $M_{\rm max}$. The mass-radius relations of hyperonic models can feature particularly small, i.e., strongly negative, curvatures in comparison to nucleonic EoSs especially for $1\ M_\odot \lesssim M \lesssim 2\ M_\odot$. Only some nucleonic models with $M_{\rm max}$ well above 2.0 $M_\odot$ can yield similarly small κ_R at larger masses above $\sim$2.0 $M_\odot$.

The small curvature for hyperonic EoSs is a consequence of the softening of the EoS at densities where hyperons occur.

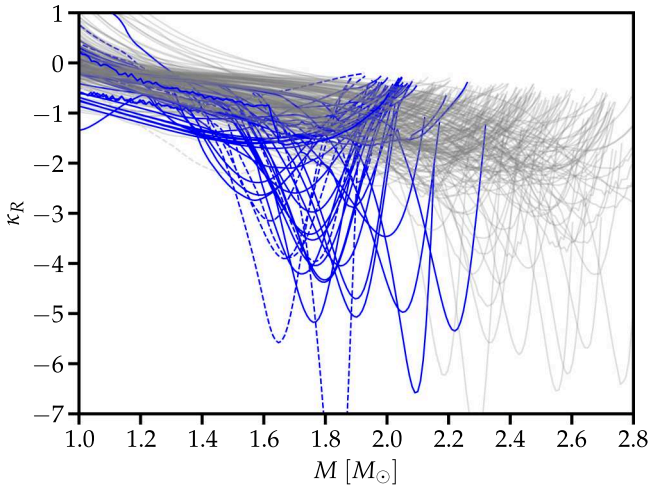

FIG. 2. Curvature κ_R as a function of mass for purely nucleonic (gray) and hyperonic (blue) EoSs. Dashed curves indicate EoSs with $M_{\max} < 2.0\,M_\odot$. For numerical reasons, the curves terminate slightly before $M_{\max}$.

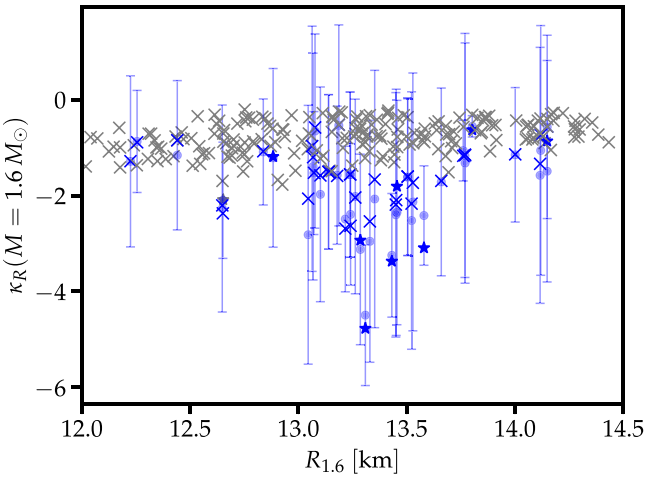

FIG. 3. Curvature κ_R evaluated at a fixed mass of 1.6 $M_\odot$ as a function of the radius $R_{1.6} = R(1.6\,M_\odot)$ for purely nucleonic (gray) and hyperonic (blue) EoSs (crosses; asterisks for EoSs with $M_{\max} < 2.0\ M_\odot$). Radius measurements at $M = 1.6\,M_\odot$ and $M = (1.6 \pm 0.25)\,M_\odot$ yield an estimate of $\kappa_R(1.6\,M_\odot)$ (dots). Error bars indicating corresponding precision for an assumed radius uncertainty of $\delta R = 100$ m (only for hyperonic models).

The mass where κ_R starts to significantly drop approximately corresponds to the onset density of hyperon production. A strongly negative curvature is found for most hyperonic EoSs of our sample although there are a few exceptions (7 out of 47 hyperonic models do not reach below $\kappa_R = -1.5$). Considering the ten hyperonic models with the smallest minima of the curvature, two models have $M_{\max} < 2.0\,M_\odot$, while eight EoSs are compatible with the constraints from pulsar measurements.

This finding suggests to measure κ_R in the range $1\ M_\odot \lesssim M \lesssim 2\ M_\odot$ to discriminate a hyperonic EoS from purely nucleonic EoSs. In particular, in the range $1.4\ M_\odot \lesssim M \lesssim 2.0\ M_\odot$ there exists no nucleonic model reaching below $\kappa_R = -2.5$. The smallest κ_R reached by nucleonic models depends on mass, and in fact the bulk of the nucleonic models does not reach below $\kappa_R = -1.5$ for $M < 2.0\ M_\odot$ (below $\kappa_R = -1.0$ for $M < 1.6\,M_\odot$). Note that κ_R not dropping below -1.5 does, however, not exclude the presence of hyperons.

A measurement of κ_R could be achieved in future by accurate radius measurements at three different masses allowing for a finite differencing estimate of the first and second derivatives of $R(M)$. We estimate the requirements for the identification of a hyperonic EoS through a determination of κ_R, where we illustrate the discussion by considering κ_R at a fixed reference mass $M_{\text{ref}} = 1.6\,M_\odot$. Analogue results can be obtained for $1.5\ M_\odot \lesssim M_{\text{ref}} \lesssim 2.1\ M_\odot$. The crosses in Fig. 3 display $\kappa_R(M = 1.6\,M_\odot)$ as a function of the radius $R_{1.6}$ of a 1.6 $M_\odot$ NS, demonstrating again the finding from Fig. 2 that hyperonic models are distinguished by particularly small curvatures.

There are two sources of error to be considered when the curvature is extracted from measurements. (1) Computing the derivatives through finite differencing requires the measurement at three different masses with the "discretization error" increasing with the step size ΔM, i.e., the difference between the masses where radii are measured. For simplicity, we here assume a constant ΔM around $M_{\text{ref}} = 1.6\ M_\odot$, i.e., measurements at $1.6\ M_\odot - \Delta M$, $1.6\ M_\odot$, and $1.6\ M_\odot + \Delta M$. (2) The radius measurements will only have a finite precision, which implies a corresponding uncertainty when the finite difference formulas are evaluated. For simplicity, we adopt the same uncertainties δR in all three measurements and neglect errors in the mass determinations, which we assume to be absorbed in the radius uncertainties.

The dots in Fig. 3 show which κ_R would be inferred for $\Delta M = 0.25\ M_\odot$ with second-order centered finite differencing. The difference between the crosses and dots quantifies the error associated with (1), and this "discretization error" remains small for $\Delta M \leqslant 0.3\ M_\odot$. For chosen ΔM and δR, we then draw error bars in Fig. 3 illustrating the error stemming from (2). Those are obtained by a standard error propagation through the finite difference formulas. In this specific example in Fig. 3 with $\Delta M = 0.25\ M_\odot$ around $M_{\text{ref}} = 1.6\ M_\odot$, an accuracy of the radius measurements of about 100 m is required to distinguish a hyperonic EoS, meaning that the corresponding error bars of certain hyperonic models hardly overlap with purely nucleonic models. The error bar grows linearly with δR but decreases with larger ΔM.

The accuracy of about 0.1 km is not yet available in current measurements, although on longer terms an order of magnitude improvement of the error might not be completely unrealistic [163–169]. We also note that statistical approaches and the inclusion of more than three measurements may improve the determination of κ_R. The exact requirements for an identification of hyperons through κ_R also depend on the considered reference mass. For instance, at masses above 1.6 $M_\odot$ the differences in κ_R between hyperonic and nucleonic models become more pronounced (Fig. 2), but obtaining measurements with sufficiently large ΔM might be less likely as one approaches $M_{\max}$.

$\frac{d^2R}{dM^2}$ at a given mass $1.5\ M_\odot \lesssim M_{\text{ref}} \lesssim 2.0\ M_\odot$ versus $R(M_{\text{ref}})$ may also be an interesting indicator for hyperons, where several hyperonic models tend to lie at lower values

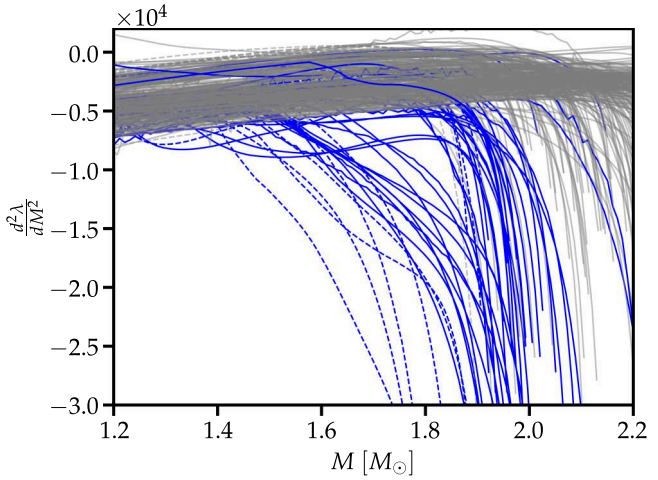

FIG. 4. Second derivative of $\lambda(M)$ with respect to mass M for hyperonic EoSs (blue) and purely nucleonic EoSs (gray). Dashed curves indicate models with $M_{\rm max} < 2.0\ M_\odot$.

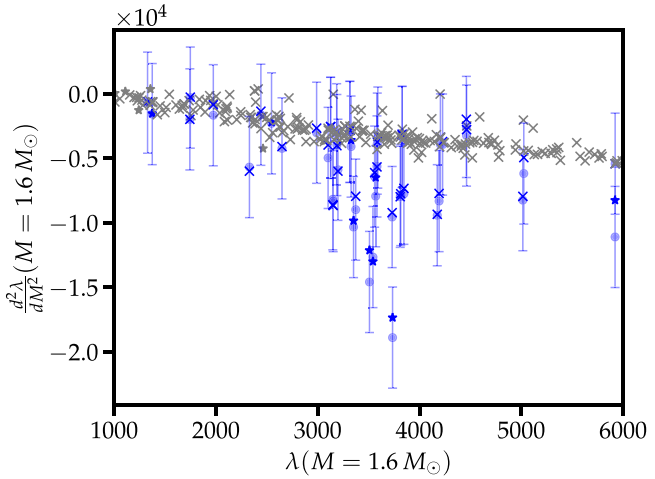

FIG. 5. Second derivative of $\lambda(M)$ with respect to mass M at fixed mass $M = 1.6\ M_\odot$ as a function of $\lambda(M = 1.6\ M_\odot)$. Symbols and colors have same meaning as in Fig. 3. See main text for details.

than purely nucleonic EoSs (similar to Fig. 3 but less pronounced; see the Appendix).

IV. TIDAL DEFORMABILITY CURVES

We now discuss the tidal deformability as indicator of hyperonic EoSs. We remark that the occurrence of features of hyperonic models in the first and second derivatives with respect to mass and the curvature κ depends on whether one considers $\lambda(M)$ or $\Lambda(M) = \lambda(M)/M^5$ because the specific effects of hyperons can cancel each other in different terms.

The imprint of hyperons becomes distinct and clear if one considers the second derivative. This occurs very prominently in Fig. 4, showing the second derivative $\frac{d^2\lambda}{dM^2}(M)$, where hyperonic models yield particularly small values for $1.4\ M_\odot \lesssim M \lesssim 1.85\ M_\odot$. At larger masses, nucleonic models can feature similarly small $\frac{d^2\lambda}{dM^2}$ as all models exhibit a decrease of $\frac{d^2\lambda}{dM^2}$ toward $M_{\rm max}$.

The potential of this signature is further demonstrated in Fig. 5 (analogue to Fig. 3). We provide an uncertainty estimate for $\frac{d^2\lambda}{dM^2}$ at $M_{\rm ref} = 1.6\ M_\odot$ with $\Delta M = 0.25\ M_\odot$. For the figure, we assume $\delta\lambda = 100$, i.e., a determination of λ within a few percent, which seems sufficient to discriminate hyperonic EoSs from purely nucleonic EoSs. Depending on the exact EoS, even larger $\delta\lambda$ could still yield evidence for hyperons in NSs noting that the uncertainty grows linearly with $\delta\lambda$. The difference between the crosses and the dots again visualizes the "discretization error," which is still acceptable for $\Delta M = 0.25\ M_\odot$. Similar figures can be obtained for other choices of the reference mass $1.4\ M_\odot \lesssim M_{\rm ref} \lesssim 1.85\ M_\odot$. For $\kappa_\lambda(M)$, i.e., the inverse curvature radius in $\lambda(M)$, we do not find features indicative of hyperonic EoSs.

It is similarly possible to consider $\Lambda(M)$, where hyperonic models do not stand out prominently in relations like $\frac{d^2\Lambda}{dM^2}(M)$ or $\kappa_\Lambda(M)$. Evaluating those quantities at fixed reference mass $1.6\ M_\odot \lesssim M_{\rm ref} \lesssim 2.0\ M_\odot$ versus $\Lambda(M_{\rm ref})$, some hyperonic models yield a characteristically reduced $\kappa_\Lambda(M_{\rm ref})$ compared to purely nucleonic EoSs, whereas $\frac{d^2\Lambda}{dM^2}(M_{\rm ref})$ is elevated (but some nucleonic models are similarly enhanced). For those hyperonic models, measurements of Λ within a few percent are sufficient to identify this signature of hyperons. However, in comparison to $\frac{d^2\lambda}{dM^2}$, the signatures are not as pronounced and especially for $\frac{d^2\Lambda}{dM^2}$ several purely nucleonic models overlap (see the Appendix).

V. SLOPES

Finally, we highlight the slopes $\frac{dR}{dM}$ and $\frac{d\Lambda}{dM}$ as indicator for hyperons (cf. Refs. [24,170–177]). Reference [24] argued that $\frac{dR}{dM} < 0$ in the range $1.2\ M_\odot \leqslant M \leqslant 1.4\ M_\odot$ would favor a nucleonic model employing statistical considerations without noting a distinctive feature for hyperonic EoSs. The slope of $R(M)$ or similarly of $\lambda(M)$ and $\Lambda(M)$ at a fixed mass on its own is not very conclusive with regards to the presence of hyperons because nucleonic models overlap over the whole range of hyperonic models (see the Appendix; with $\frac{d\lambda}{dM}$ appearing slightly more promising).

We, however, point out that comparing the slopes at a fixed mass to the maximum mass, some specific hyperonic models stand out clearly. Figure 6 shows $\frac{dR}{dM}$ and $\frac{d\Lambda}{dM}$ evaluated at $M_{\rm ref} = 1.6\ M_\odot$ as a function of $M_{\rm max}$ demonstrating that an increased (decreased) slope in $\frac{dR}{dM}$ ($\frac{d\Lambda}{dM}$) compared to $M_{\rm max}$ is a distinctive feature of hyperonic models. For $\frac{d\Lambda}{dM}$ there are, however, two nucleonic models with similarly small slope. For $\frac{d\lambda}{dM}$, hyperonic EoSs do not occur distinguished. Similar findings hold for $1.2\ M_\odot \lesssim M_{\rm ref} \lesssim 1.8\ M_\odot$. At first glance, an increased slope of $R(M)$ may seem counterintuitive as indicator of hyperons as one would associate it with a certain stiffness of the EoS. In those models, hyperons soften the EoS at higher densities and thus reduce $M_{\rm max}$ more strongly than any purely nucleonic model with the same slope.

Measuring a slope can be assessed by assuming measurements for NSs with two masses separated by ΔM. Employing second-order finite differencing, the uncertainty in the slope is given by $\sqrt{2}\frac{\delta R}{\Delta M}$ and $\sqrt{2}\frac{\delta\Lambda}{\Delta M}$, respectively, neglecting the discretization error, which is very small for $\Delta M \sim 0.2\ M_\odot$

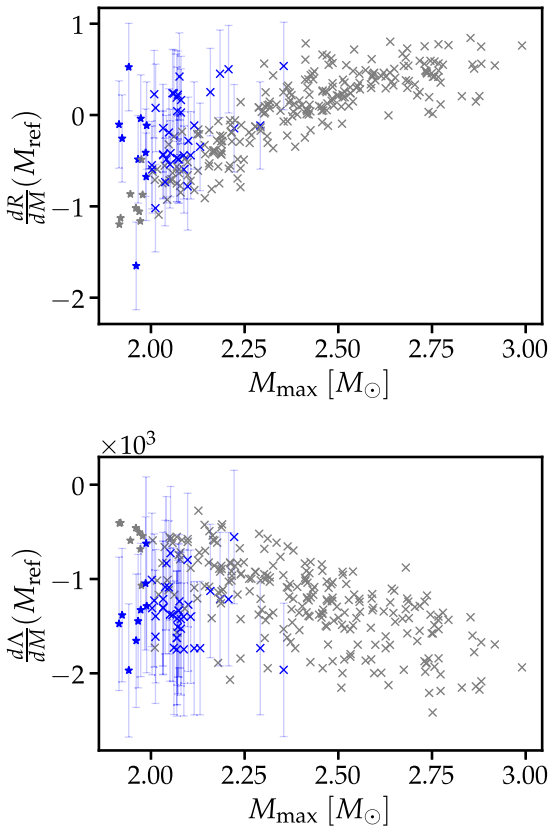

FIG. 6. Slope of $R(M)$ (top) and $\Lambda(M)$ (bottom) at a fixed mass of $M_{\rm ref} = 1.6\ M_\odot$ as a function of the maximum mass of NS. Symbols and colors have the same meaning as in Fig. 3 with error bars computed for the values mentioned in the main text.

and $M_{\rm ref} \sim 1.6\ M_\odot$. The scales in Fig. 6 suggest that $\delta R \sim 0.1$ km or $\delta\Lambda \sim 100$ (about 10% level) is sufficient with $\Delta M = 0.2\ M_\odot$ to identify hyperons. While these demands on measurements look relatively promising especially for the tidal deformability, the identification of hyperons via these features also requires a solid upper bound on $M_{\rm max}$, which may not be easily available.

VI. DISCUSSION AND OUTLOOK

We describe stellar features that allow to quantitatively distinguish a hyperonic EoS from purely nucleonic EoSs. Requirements for corresponding measurements are generally challenging but not completely out of reach [163–169]. In particular, the required precision for measurements of the tidal deformability of a few percent might be feasible with the next generation of GW detectors [45,47] although this precision has to be achieved for high-mass NSs. Future work should thus explore the capabilities of new instruments [45–48] and the potential of statistical methods including, for instance, more than three measurements.

The effects described in this study are generally associated with a softening of the EoS, which goes beyond what a purely nucleonic EoS may attain, and we did not explicitly consider other non-nucleonic degrees of freedom (apart from Δ resonances being considered in some of the hyperonic models). A transition to quark matter might mimic the behavior of hyperonic models and would thus need to be further discriminated by additional information, e.g., from experiments like heavy-ion collisions, NS cooling, or NS mergers (e.g., Refs. [7,13,18,26–36,52,53,178–181]). If quark matter occurs via a first-order phase transition (as opposed to the rather smooth appearance of hyperons), a characteristic kink or even discontinuity in the mass-radius relation is present [1,2,6]. Future work should also elaborate on which particular properties of hyperonic matter lead to pronounced features, while some hyperonic models do not exhibit prominent differences compared to purely nucleonic EoSs. A refined study may disregard some of the nucleonic models of our sample by imposing further experimental or theoretical constraints, by which hyperonic EoSs may stand out even more clearly in the discussed relations.

ACKNOWLEDGMENTS

We thank David Blaschke, Gabriel Martinez-Pinedo, and Angels Ramos for helpful discussions, and Hui Tong for providing EoS tables. A.B. and A.N. acknowledge support by the European Union through ERC Synergy Grant HeavyMetal, Grant No. 101071865. A.B. acknowledges support by Deutsche Forschungsgemeinschaft (DFG, German Research Foundation) through Project-ID 279384907—SFB 1245 (Subproject No. B07). G.L. acknowledges support by the Klaus Tschira Foundation. This project has received funding from the European Union's Horizon 2020 research and innovation programme under the Marie Skłodowska-Curie Grant Agreement No. 101034371. P.C. acknowledges the support from the European Union's HORIZON MSCA-2022-PF-01-01 Programme under Grant Agreement No. 101109652, project ProMatEx-NS. C.M. acknowledges partial support from the Fonds de la Recherche Scientifique (FNRS, Belgium) and the Research Foundation Flanders (FWO, Belgium) under the EOS Projects No. O022818F and No. O000422. M.O. acknowledges financial support of the Agence Nationale de la Recherche (ANR) under Contract No. ANR-22-CE31-0001-01. L.T. acknowledges support from the program Unidad de Excelencia María de Maeztu CEX2020-001058-M, from the Project No. PID2022-139427NB-I00 financed by the Spanish MCIN/AEI/10.13039/501100011033/FEDER, UE (FSE+), from the Grant CIPROM 2023/59 of Generalitat Valenciana and from CRC-TR 211 "Strong-interaction matter under extreme conditions," Project No. 315477589—TRR 211 by the Deutsche Forschungsgemeinshaft. S.G. and N.C. acknowledge financial support from F.R.S.-FNRS (Belgium). This work was supported by the Fonds de la Recherche Scientifique—FNRS and the Fonds Wetenschappelijk Onderzoek—Vlaanderen (FWO) under the EOS Project No. O000422.

DATA AVAILABILITY

The data that support the findings of this article are not publicly available. The data are available from the authors upon reasonable request.

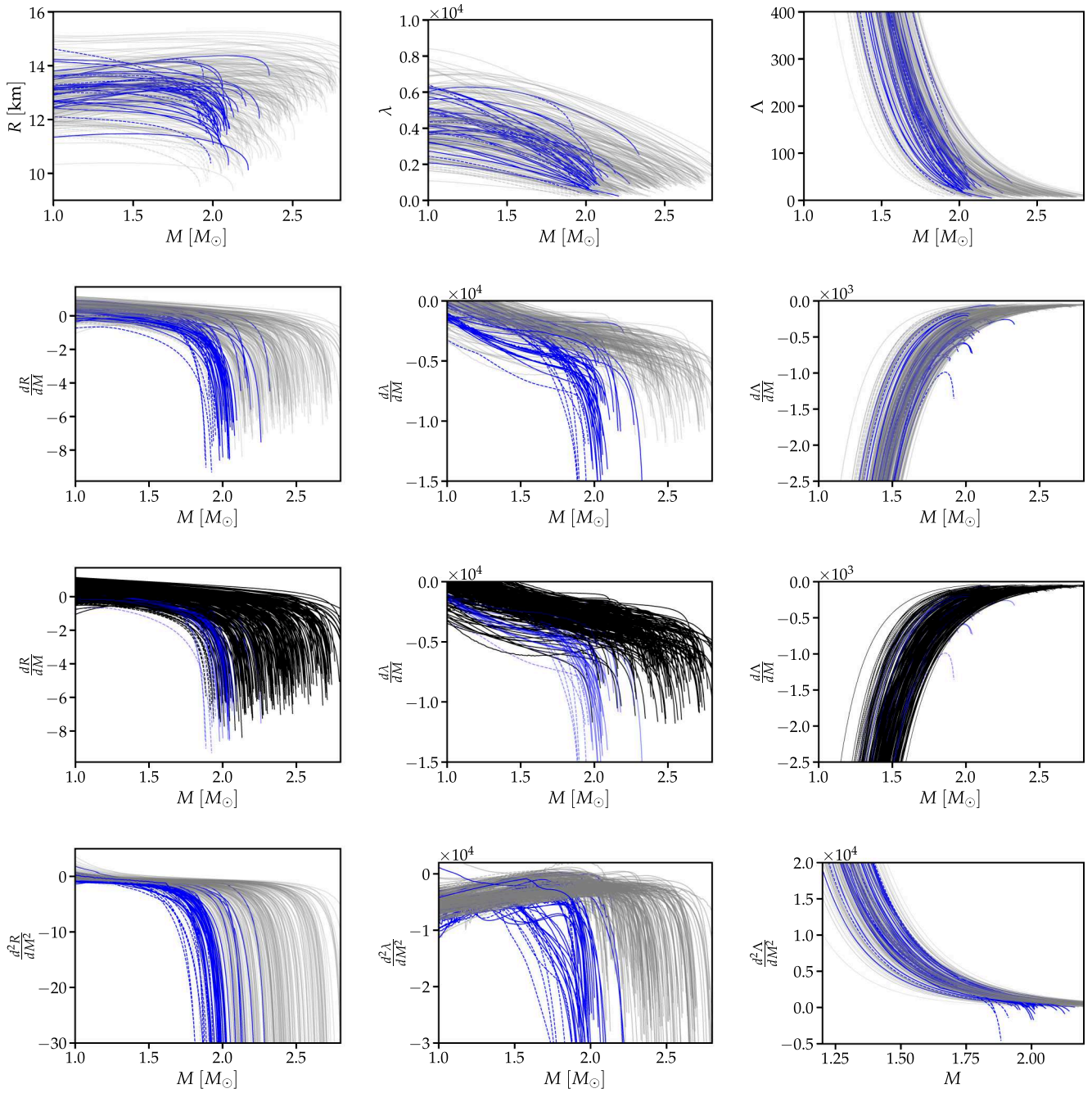

FIG. 7. Upper panels: Stellar parameters of NSs as a function of mass with the radius (left), the tidal deformability λ (middle), and the mass-scaled tidal deformability $\Lambda = \lambda/M^5$ (right). The latter two quantities are dimensionless or in geometric units, respectively. Purely nucleonic models are displayed in gray, while models with hyperons are highlighted in blue. Dashed curves indicate models with $M_{\max} < 2.0\ M_\odot$. Second-row panels: First derivatives with respect to mass of the respective quantity of the panel above. The same line scheme as in the upper panels is applied. Third-row panels: Same as second row but with purely nucleonic models visually more emphasized by black curves to assess overlap between hyperonic and purely nucleonic EoSs. Lower panels: Second derivatives with respect to mass of the respective quantity of the upper panel.

APPENDIX: EOS MODELS AND ADDITIONAL PLOTS

We list all EoS models used in this study in Table I along with the respective references and some stellar parameters.

The solutions from the stellar structure equations [8–12] determining R, λ, and $\Lambda = \lambda/M^5$ are shown in Fig. 7. If necessary, we extend the EoS tables to smaller densities by adding a crust EoS [92,102] such that the integration terminates at $P \approx 3 \times 10^{14}\,\mathrm{dyne/cm^2}$ for all models [182]. The figure also provides the first and second derivatives with respect to mass. We obtain these derivatives by numerical differentiation using a centered second-order finite difference formula with variable step size. We note that numerical values of the derivatives or κ_R can be noisy depending on the details and accuracy of the Tolman-Oppenheimer-Volkoff (TOV) solutions, which can be cured by using larger step

TABLE I. EoS models employed in this work. Columns provide EoS acronym, maximum mass ($M_{\max}$), radius and dimensionless tidal deformability at 1.6 $M_\odot$ ($R_{1.6}$ and $\Lambda_{1.6}$, respectively), presence of hyperons, and references to the EoS.

EoS	$M_{\max}$ ($M_\odot$)	$R_{1.6}$ (km)	$\Lambda_{1.6}$	Hyperons	Reference
DDLS(30)-N	2.48	13.06	325.4	No	[90]
DDLS(30)-Y	2.01	13.04	321.7	Yes	[90]
DDLS(50)-N	2.47	13.32	327.8	No	[90]
DDLS(50)-Y	1.99	13.29	319.7	Yes	[90]
DDLS(70)-N	2.46	13.64	352.1	No	[90]
DDLS(70)-Y	1.97	13.58	337.9	Yes	[90]
Bonn1	2.23	12.44	188.3	No	[91,92]
Bonn2	2.04	12.44	188.3	Yes	[91,92]
DNS	2.09	14.0	403.2	Yes	[75]
DSH fiducial	2.17	11.67	121.3	No	[87]
DSH large M_{max}	2.21	12.67	222.9	No	[87]
DSH large SL	2.16	11.66	110.0	No	[87]
DSH large R	2.12	12.34	175.3	No	[87]
DSH small SL	2.18	11.69	138.4	No	[87]
DSH smaller R	2.14	11.26	96.0	No	[87]
FSU2H*L	1.92	13.31	356.2	Yes	[89]
FSU2H*U	2.06	13.35	366.9	Yes	[89]
FSU2H*	2.01	13.33	355.9	Yes	[88]
FSU2R	2.06	12.93	275.2	No	[76]
FTNS	2.22	11.46	126.7	Yes	[77,78]
LPB	2.1	12.26	166.7	Yes	[82,84]
QMC-A	1.99	12.88	242.8	Yes	[85]
SRO(SLy4)	2.06	11.57	116.4	No	[62,79]
BHBLP	2.1	13.26	305.1	Yes	[73]
DD2	2.42	13.32	317.5	No	[68,69]
DD2Y	2.03	13.24	300.3	Yes	[80,81]
DD2F	2.08	12.24	165.6	No	[65,69,74]
WFF1	2.13	10.37	60.7	No	[56]
WFF2	2.19	11.07	92.8	No	[56]
BSK20	2.17	11.66	129.5	No	[57]
BSK21	2.28	12.55	223.3	No	[57]
LS220	2.04	12.54	203.6	No	[58]
LS375	2.71	13.84	446.0	No	[58]
GS1	2.75	14.96	649.2	No	[71]
GS2	2.09	13.44	308.5	No	[71]
ALF2	1.98	12.65	234.9	No	[64,67]
AP3	2.37	11.97	159.3	No	[63,67]
ENG	2.24	11.91	153.3	No	[61,67]
GNH3	1.96	13.8	317.4	Yes	[54,67]
H4	2.01	13.76	341.7	Yes	[66,67]
MPA1	2.46	12.46	213.9	No	[55,67]
SFHO	2.06	11.8	131.4	No	[72]
SFHOY	1.99	11.8	131.1	Yes	[80,81]
SFHX	2.13	12.02	167.3	No	[72]
SkAPR	2.03	12.37	176.3	No	[58,79,83]
TM1	2.21	14.43	488.1	No	[59,70]
TMA	2.01	13.69	376.3	No	[60,70]
ABHT(QMC-RMF1)	1.95	11.66	118.4	No	[92,118,146,147]
ABHT(QMC-RMF2)	2.04	11.90	142.8	No	[92,118,146,147]
ABHT(QMC-RMF3)	2.15	12.15	159.6	No	[92,118,146,147]
ABHT(QMC-RMF4)	2.21	12.35	201.6	No	[92,118,146,147]
APR	2.19	11.26	100.7	No	[63,92,102]
BBB(BHF-BBB2)	1.92	10.86	72.4	No	[92,101,102]
BL(chiral) w. un. crust	2.08	12.10	147.1	No	[82,148,156]
CMGO(GDFM-II)	2.30	13.89	431.1	No	[145,148]
CMGO(GDFM-I)	2.31	12.80	233.8	No	[145,148]
DNS(CMF)	2.07	13.51	365.3	Yes	[112,114,120,121]
DS(CMF-1-ybrid)	2.07	13.50	365.3	Yes	[75,112,113,128,136,141]

TABLE I. (*Continued.*)

EoS	$M_{\max}$ ($M_\odot$)	$R_{1.6}$ (km)	$\Lambda_{1.6}$	Hyperons	Reference
DS(CMF-2-Hybrid)	2.13	13.66	401.1	Yes	[75,112,113,128,136,141]
DS(CMF-3-Hybrid)	2.00	13.07	285.1	Yes	[75,112,113,128,136,141]
DS(CMF-4-Hybrid)	2.05	13.18	303.9	Yes	[75,112,113,128,136,141]
DS(CMF-5-Hybrid)	2.07	13.14	298.3	Yes	[75,112,113,128,136,141]
DS(CMF-6-Hybrid)	2.11	13.24	316.3	Yes	[75,112,113,128,136,141]
DS(CMF-7-Hybrid)	2.07	13.14	298.3	Yes	[75,112,113,128,136,141]
DS(CMF-8-Hybrid)	2.09	13.24	316.3	Yes	[75,112,113,128,136,141]
GDTB(DDHdelta)	2.16	12.65	253.0	No	[102,105,118]
GM(GM1)	2.39	14.11	425.8	No	[97,102]
GMSR(BSK14)	1.92	10.88	72.3	No	[140]
GMSR(DHSL59)	2.43	12.47	199.7	No	[140]
GMSR(DHSL69)	2.41	12.51	200.2	No	[140]
GMSR(F0)	2.07	11.55	117.2	No	[140]
GMSR(H1)	2.29	11.51	129.1	No	[140]
GMSR(H2)	2.31	11.71	144.1	No	[140]
GMSR(H3)	2.30	12.04	169.4	No	[140]
GMSR(H4)	2.34	11.87	156.5	No	[140]
GMSR(H5)	2.38	12.17	180.5	No	[140]
GMSR(H7)	2.51	12.85	251.1	No	[140]
GMSR(LNS5)	1.98	11.41	105.9	No	[140]
GMSR(SLy5)	2.10	11.63	120.1	No	[140]
GPPVA(DD2)	2.42	13.22	311.6	No	[69,118,126]
GPPVA(DDME2)	2.48	13.30	328.1	No	[107,118,126]
GPPVA(FSU2)	2.07	13.71	346.8	No	[118,126,149,150]
GPPVA(FSU2H)	2.38	13.38	354.7	No	[29,118,126,149]
GPPVA(FSU2R)	2.05	12.91	260.5	No	[29,118,126,149]
GPPVA(NL3wrL55)	2.75	13.87	451.8	No	[118,126,151]
GPPVA(TM1e)	2.12	13.14	292.3	No	[118,126,152]
GPPVA(TW)	2.08	12.18	161.0	No	[100,118,126]
OPGR(DD2HdeltaY4)	2.05	12.65	252.7	Yes	[102,105,118,119]
OPGR(GM1Y5)	2.12	13.77	425.6	Yes	[97,102,119]
OPGR(GM1Y6)	2.29	13.77	425.5	Yes	[97,102,119]
PCGS(PCSB0)	2.53	13.34	324.3	No	[68,138,143]
PCGS(PCSB1)	2.19	13.04	269.8	No	[68,143]
PCGS(PCSB2)	2.02	12.76	225.2	No	[68,143]
PCP(BSK22)	2.26	12.98	266.3	No	[116,117,122,123,126,129,130,135,142]
PCP(BSK24)	2.28	12.56	224.1	No	[116,117,122,123,126,129,130,135,142]
PCP(BSK25)	2.22	12.39	210.2	No	[116,117,122,123,126,129,130,135,142]
PCP(BSK26)	2.17	11.69	131.5	No	[116,117,122,123,126,129,130,135,142]
PT(GRDF2-DD2)	2.42	13.20	309.8	No	[69,124,127]
R(DD2YDelta) 1.1-1.1	2.04	12.84	232.9	Yes	[5,69,131,137]
R(DD2YDelta) 1.2-1.3	2.03	13.22	300.6	Yes	[5,69,131,137]
R(DD2YDelta) 1.2-1.1	2.05	12.22	166.3	Yes	[5,69,131,137]
RG(KDE0v)	1.96	11.19	86.9	No	[110,111,121]
RG(KDE0v1)	1.97	11.38	96.1	No	[110,111,121]
RG(Rs)	2.12	12.75	227.0	No	[94,111,121]
RG(SK255)	2.14	12.93	227.0	No	[104,111,121]
RG(SK272)	2.23	13.15	259.2	No	[104,111,121]
RG(SKI2)	2.16	13.31	300.7	No	[98,111,121]
RG(SKa)	2.21	12.79	228.0	No	[93,111,121]
RG(SKb)	2.19	12.18	192.5	No	[93,111,121]
RG(SLY2)	2.05	11.63	118.7	No	[111,121]
RG(SLY2)	2.10	11.73	131.2	No	[111,121]
RG(SLY4)	2.05	11.55	114.0	No	[62,111,121]
RG(SLY9)	2.15	12.35	181.0	No	[111,121]
RG(SkI3)	2.24	13.44	321.0	No	[98,111,121]
RG(SkI4)	2.17	12.31	191.0	No	[98,111,121]
RG(SkI5)	2.24	13.91	400.9	No	[98,111,121]
RG(SkI6)	2.19	12.42	201.4	No	[98,111,121]

TABLE I. (*Continued.*)

EoS	$M_{\max}$ ($M_\odot$)	$R_{1.6}$ (km)	$\Lambda_{1.6}$	Hyperons	Reference
RG(SkMp)	2.11	12.34	184.8	No	[96,111,121]
RG(SkOp)	1.97	11.86	129.4	No	[95,111,121]
SPG(M1)	2.54	12.83	247.4	No	[126,153]
SPG(M2)	2.42	12.65	234.8	No	[126,153]
SPG(M3)	2.68	12.75	249.8	No	[126,153]
SPG(M4)	2.35	12.31	194.3	No	[126,153]
SPG(M5)	2.70	13.50	365.4	No	[126,153]
VGBCMR(D1M)	2.01	11.58	122.4	No	[125,132,137]
XMLSLZ(DD-LZ1)	2.56	13.26	344.2	No	[133,139]
XMLSLZ(DDMEX)	2.56	13.46	369.3	No	[134,139]
XMLSLZ(DDME2)	2.48	13.26	329.5	No	[107,139]
XMLSLZ(GM1)	2.36	13.71	393.0	No	[97,139]
XMLSLZ(MTVTC)	2.02	12.83	230.4	No	[108,139]
XMLSLZ(NL3)	2.77	14.62	591.0	No	[99,139]
XMLSLZ(PK1)	2.31	14.29	478.9	No	[106,139]
XMLSLZ(PKDD)	2.33	13.54	326.8	No	[106,139]
XMLSLZ(TM1)	2.18	14.14	437.8	No	[59,139]
XMLSLZ(TW99)	2.08	12.13	161.0	No	[100,139]
eos1	2.21	13.08	341.9	Yes	[155,156]
eos2	1.94	14.15	564.8	Yes	[155,156]
eos3	2.06	14.12	479.2	Yes	[155,156]
eos4	2.07	13.45	363.9	Yes	[155,156]
eos5	2.07	13.53	399.8	Yes	[155,156]
eos6	1.92	13.43	334.7	Yes	[155,156]
eos7	2.03	13.10	295.9	Yes	[155,156]
eos9	2.00	12.65	222.2	Yes	[155,156]
eos0	2.18	13.19	342.4	Yes	[155,156]
eos1	2.08	13.07	339.5	Yes	[155,156]
eos2	2.35	14.15	564.8	Yes	[155,156]
eos3	2.07	14.12	478.3	Yes	[155,156]
eos4	2.08	13.45	363.4	Yes	[155,156]
eos5	2.08	13.52	398.1	Yes	[155,156]
eos6	1.97	13.45	340.4	Yes	[155,156]
eos8	2.16	13.06	304.1	Yes	[155,156]
eos0	2.56	13.19	342.4	No	[145,156]
eos7	2.29	13.10	295.8	No	[145,156]
(GDFM)eos1	2.36	12.89	292.7	No	[145,156]
(GDFM)eos3	2.30	12.63	271.9	No	[145,156]
(GDFM)eos6	2.26	12.75	240.3	No	[145,156]
(GDFM)eos8	2.51	14.38	549.8	No	[145,156]
(GDFM)eos11	2.92	14.18	510.1	No	[145,156]
(GDFM)eos12	2.45	13.70	372.3	No	[145,156]
(GDFM)eos15	2.72	14.17	446.5	No	[145,156]
(GDFM)eos19	2.27	12.74	238.4	No	[145,156]
(GDFM)eos20	2.65	13.63	384.4	No	[145,156]
(GDFM)eos22	2.74	14.94	629.6	No	[145,156]
(GDFM)eos24	2.51	14.15	401.3	No	[145,156]
(GDFM)eos28	2.18	12.69	214.1	No	[145,156]
(GDFM)eos30	2.87	15.16	624.8	No	[145,156]
(GDFM)eos36	2.46	13.57	351.3	No	[145,156]
(GDFM)eos39	2.51	14.65	583.8	No	[145,156]
(GDFM)eos41	2.52	13.76	428.5	No	[145,156]
(GDFM)eos43	2.77	13.86	449.0	No	[145,156]
(GDFM)eos45	2.77	13.74	414.8	No	[145,156]
(GDFM)eos48	2.19	13.11	264.9	No	[145,156]
(GDFM)eos50	2.18	12.87	201.1	No	[145,156]
(GDFM)eos52	2.08	11.66	135.8	No	[145,156]
(GDFM)eos58	2.65	13.87	424.6	No	[145,156]
(GDFM)eos60	2.63	14.06	456.8	No	[145,156]

TABLE I. (*Continued.*)

EoS	$M_{\max}$ ($M_\odot$)	$R_{1.6}$ (km)	$\Lambda_{1.6}$	Hyperons	Reference
(GDFM)eos61	2.47	14.30	448.7	No	[145,156]
(GDFM)eos64	2.18	12.99	282.7	No	[145,156]
(GDFM)eos66	2.74	14.87	528.8	No	[145,156]
(GDFM)eos67	2.73	14.28	552.6	No	[145,156]
(GDFM)eos72	2.88	15.18	642.1	No	[145,156]
(GDFM)eos78	2.88	14.53	621.8	No	[145,156]
(GDFM)eos80	2.49	13.82	391.5	No	[145,156]
(GDFM)eos82	2.77	14.12	540.5	No	[145,156]
(GDFM)eos84	2.83	15.03	625.8	No	[145,156]
(GDFM)eos85	2.63	15.02	593.5	No	[145,156]
(GDFM)eos89	2.19	13.44	301.4	No	[145,156]
(GDFM)eos92	2.77	14.61	584.4	No	[145,156]
(GDFM)eos94	2.24	12.51	241.1	No	[145,156]
(GDFM)eos10	2.55	14.09	479.2	No	[145,156]
(GDFM)eos17	2.74	13.41	346.0	No	[145,156]
(GDFM)eos54	2.44	12.88	304.4	No	[145,156]
(GDFM)eos73	2.37	14.05	455.6	No	[145,156]
(GDFM)eos99	2.33	12.32	233.0	No	[145,156]
eos101	2.59	13.72	422.5	No	[145,156]
eos102	2.47	12.77	301.0	No	[145,156]
eos103	2.53	13.68	420.6	No	[145,156]
eos105	2.59	13.16	327.7	No	[145,156]
eos106	2.62	13.40	381.4	No	[145,156]
eos108	2.59	13.29	366.8	No	[145,156]
eos109	2.75	13.85	454.9	No	[145,156]
eos110	2.39	13.02	277.4	No	[145,156]
eos111	2.32	13.31	355.5	No	[145,156]
eos112	2.64	13.16	311.6	No	[145,156]
eos114	2.38	13.21	311.5	No	[145,156]
eos117	2.35	12.65	254.3	No	[145,156]
eos118	2.50	13.58	382.3	No	[145,156]
eos119	2.40	13.30	335.8	No	[145,156]
eos122	2.61	14.28	566.2	No	[145,156]
eos125	2.41	12.62	289.9	No	[145,156]
eos126	2.74	14.32	551.9	No	[145,156]
eos128	2.54	13.58	423.9	No	[145,156]
eos13	2.57	14.05	532.0	No	[145,156]
eos130	2.69	13.65	400.9	No	[145,156]
eos131	2.60	14.27	571.5	No	[145,156]
eos132	2.42	12.66	248.3	No	[145,156]
eos133	2.40	13.33	349.4	No	[145,156]
eos135	2.68	13.91	441.6	No	[145,156]
eos138	2.88	13.80	506.3	No	[145,156]
eos14	2.64	13.89	483.4	No	[145,156]
eos144	2.32	12.59	250.0	No	[145,156]
eos147	2.51	12.76	266.5	No	[145,156]
eos149	2.42	12.70	275.2	No	[145,156]
eos158	2.53	14.06	489.1	No	[145,156]
eos16	2.60	13.85	471.4	No	[145,156]
eos160	2.72	13.27	374.9	No	[145,156]
eos161	2.22	12.74	243.9	No	[145,156]
eos162	2.43	12.94	317.0	No	[145,156]
eos166	2.47	13.57	403.9	No	[145,156]
eos168	2.53	14.13	499.3	No	[145,156]
eos171	2.41	12.61	266.9	No	[145,156]
eos173	2.64	13.11	379.5	No	[145,156]
eos175	2.21	12.25	198.8	No	[145,156]
eos176	2.47	12.86	311.1	No	[145,156]
eos178	2.30	12.69	251.1	No	[145,156]

TABLE I. (*Continued.*)

EoS	$M_{\max}$ ($M_\odot$)	$R_{1.6}$ (km)	$\Lambda_{1.6}$	Hyperons	Reference
eos179	2.59	13.28	370.2	No	[145,156]
eos18	2.77	13.33	421.0	No	[145,156]
eos182	2.79	13.41	432.4	No	[145,156]
eos186	2.68	13.19	367.0	No	[145,156]
eos188	2.47	13.26	316.2	No	[145,156]
eos191	2.46	14.27	536.7	No	[145,156]
eos193	2.52	13.46	363.5	No	[145,156]
eos196	2.48	12.75	303.7	No	[145,156]
eos198	2.48	12.79	297.0	No	[145,156]
eos2	2.67	14.15	564.8	No	[145,156]
eos200	2.55	13.68	395.5	No	[145,156]
eos203	2.31	13.39	380.6	No	[145,156]
eos207	2.52	14.08	504.9	No	[145,156]
eos208	2.59	13.16	354.5	No	[145,156]
eos211	2.43	13.05	331.3	No	[145,156]
eos213	2.59	14.12	510.3	No	[145,156]
eos216	2.75	13.46	404.7	No	[145,156]
eos223	2.42	13.51	351.3	No	[145,156]
eos224	2.63	14.06	496.5	No	[145,156]
eos23	2.46	13.58	371.6	No	[145,156]
eos231	2.46	13.50	373.9	No	[145,156]
eos232	2.65	13.05	322.3	No	[145,156]
eos234	2.52	12.72	296.1	No	[145,156]
eos26	2.30	13.38	341.7	No	[145,156]
eos27	2.67	13.36	416.8	No	[145,156]
eos29	2.78	13.49	397.3	No	[145,156]
eos33	2.18	13.15	294.6	No	[145,156]
eos35	2.35	13.68	387.3	No	[145,156]
eos37	2.40	13.73	411.3	No	[145,156]
eos4	2.42	13.46	365.1	No	[145,156]
eos42	2.41	12.61	300.6	No	[145,156]
eos46	2.29	13.25	348.6	No	[145,156]
eos47	2.37	13.08	308.5	No	[145,156]
eos49	2.48	14.08	513.5	No	[145,156]
eos5	2.47	13.53	400.4	No	[145,156]
eos53	2.43	14.17	492.0	No	[145,156]
eos54	2.37	12.73	288.5	No	[145,156]
eos55	2.76	13.83	431.2	No	[145,156]
eos56	2.46	12.53	268.3	No	[145,156]
eos57	2.50	13.36	348.4	No	[145,156]
eos59	2.69	13.31	362.4	No	[145,156]
eos63	2.38	13.65	376.7	No	[145,156]
eos65	2.73	13.20	377.1	No	[145,156]
eos68	2.24	12.55	227.3	No	[145,156]
eos69	2.76	14.18	566.6	No	[145,156]
eos71	2.43	12.93	310.7	No	[145,156]
eos76	2.32	12.67	258.0	No	[145,156]
eos77	2.37	12.70	273.8	No	[145,156]
eos78	2.85	13.42	435.4	No	[145,156]
eos79	2.29	12.87	248.7	No	[145,156]
eos81	2.86	13.88	472.0	No	[145,156]
eos83	2.99	14.22	595.6	No	[145,156]
eos87	2.73	14.36	577.6	No	[145,156]
eos88	2.68	13.27	385.3	No	[145,156]
eos9	2.22	12.68	227.5	No	[145,156]
eos91	2.42	13.38	383.4	No	[145,156]
eos93	2.54	12.97	345.4	No	[145,156]
eos97	2.86	14.01	512.0	No	[145,156]
eos98	2.73	14.11	545.6	No	[145,156]

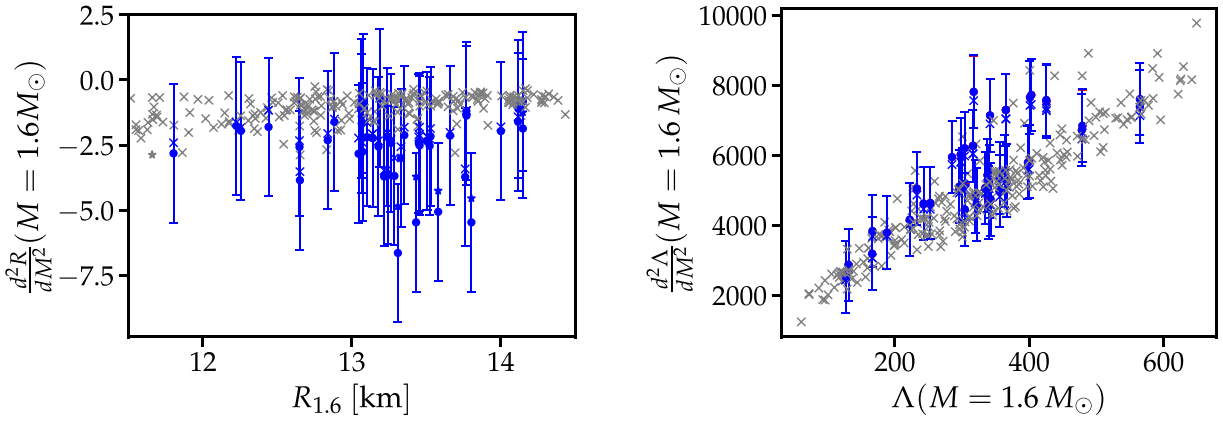

FIG. 8. Second derivative of $R(M)$ (left) and $\Lambda(M)$ (right) with respect to mass M at a fixed reference mass $M = 1.6\,M_\odot$ as a function of $R(M = 1.6\,M_\odot)$ (left) and $\Lambda(M = 1.6\,M_\odot)$, respectively. Symbols have the same meaning as in Fig. 3 of the main paper. We adopt $\delta R = 100$ m and $\Delta M = 0.25\,M_\odot$ for the left panel and $\delta\Lambda = 100/1.6^5$ and $\Delta M = 0.15\,M_\odot$ for the right panel. See main text for more details.

sized for the finite differences (without effects on the smooth behavior of the curves). The panels in the third row display data that are identical to those in the second row but using a different color scheme to better visualize different purely nucleonic models. By this, the overlap between hyperonic and purely nucleonic models becomes more apparent.

Figure 8 shows $\frac{d^2R}{dM^2}(M)$ and $\frac{d^2\Lambda}{dM^2}(M)$ at a fixed reference mass $M = 1.6\,M_\odot$ similar to Figs. 3 and 5. For the right panel, we adopt $\Delta = 0.15\ M_\odot$ because the discretization errors become comparable to errors stemming from the finite precision in Λ if $\Delta = 0.25\ M_\odot$ is used.

[1] N. K. Glendenning, *Compact Stars: Nuclear Physics, Particle Physics and General Relativity*, Astronomy and Astrophysics Library (Springer, New York, 1997).

[2] P. Haensel, A. Y. Potekhin, and D. G. Yakovlev, *Neutron Stars 1: Equation of State and Structure* (Springer, New York, 2007), Vol. 326.

[3] J. M. Lattimer and M. Prakash, The equation of state of hot, dense matter and neutron stars, Phys. Rep. **621**, 127 (2016).

[4] G. Baym, T. Hatsuda, T. Kojo, P. D. Powell, Y. Song, and T. Takatsuka, From hadrons to quarks in neutron stars: A review, Rep. Prog. Phys. **81**, 056902 (2018).

[5] A. R. Raduta, Equations of state for hot neutron stars—II. The role of exotic particle degrees of freedom, Eur. Phys. J. A **58**, 115 (2022).

[6] J. Schaffner-Bielich, *Compact Star Physics* (Cambridge University Press, Cambridge, UK, 2020).

[7] R. Kumar, *et al.*, Theoretical and experimental constraints for the equation of state of dense and hot matter, Living Rev. Relativ. **27**, 3 (2024).

[8] R. C. Tolman, Static solutions of Einstein's field equations for spheres of fluid, Phys. Rev. **55**, 364 (1939).

[9] J. R. Oppenheimer and G. M. Volkoff, On massive neutron cores, Phys. Rev. **55**, 374 (1939).

[10] T. Hinderer, Tidal Love numbers of neutron stars, Astrophys. J. **677**, 1216 (2008).

[11] T. Binnington and E. Poisson, Relativistic theory of tidal Love numbers, Phys. Rev. D **80**, 084018 (2009).

[12] T. Hinderer, B. D. Lackey, R. N. Lang, and J. S. Read, Tidal deformability of neutron stars with realistic equations of state and their gravitational wave signatures in binary inspiral, Phys. Rev. D **81**, 123016 (2010).

[13] A. Gal, E. V. Hungerford, and D. J. Millener, Strangeness in nuclear physics, Rev. Mod. Phys. **88**, 035004 (2016).

[14] Nuclear Science Advisory Committee, A new era of discovery—The 2023 long range plan for nuclear physics (2023).

[15] NuPECC (Nuclear Physics European Collaboration Committee), NuPECC long range plan 2024 for european nuclear physics, arXiv:2503.15575.

[16] CompOSE Core Team, S. Typel, M. Oertel, T. Klähn, D. Chatterjee, V. Dexheimer, C. Ishizuka, M. Mancini, J. Novak, H. Pais, C. Providência, A. R. Raduta, M. Servillat, and L. Tolos, CompOSE reference manual, Eur. Phys. J. A **58**, 221 (2022).

[17] G. F. Burgio, H. J. Schulze, I. Vidana, and J. B. Wei, Neutron stars and the nuclear equation of state, Prog. Part. Nucl. Phys. **120**, 103879 (2021).

[18] A. Sedrakian, J.-J. Li, and F. Weber, Heavy baryons in compact stars, Prog. Part. Nucl. Phys. **131**, 104041 (2023).

[19] A. Sedrakian, J.-J. Li, and F. Weber, *Astrophysics in the XXI Century with Compact Stars.* (World Scientific, Singapore, 2022), pp. 153–199.

[20] L. Tolos and L. Fabbietti, Strangeness in nuclei and neutron stars, Prog. Part. Nucl. Phys. **112**, 103770 (2020).

[21] D. Chatterjee and I. Vidaña, Do hyperons exist in the interior of neutron stars? Eur. Phys. J. A **52**, 29 (2016).

[22] I. Vidaña, Hyperons: The strange ingredients of the nuclear equation of state, Proc. A **474**, 20180145 (2018).

[23] D. Logoteta, Hyperons in neutron stars, Universe **7**, 408 (2021).
[24] M. Ferreira and C. Providência, Learning about neutron star composition from the slope of the mass-radius diagram, Phys. Rev. D **112**, 083058 (2025).
[25] C. Huang, L. Tolos, C. Providência, and A. Watts, Constraining a relativistic mean field model using neutron star mass-radius measurements II: Hyperonic models, Mon. Not. R. Astron. Soc. **536**, 3262 (2025).
[26] D. Page and E. Baron, Strangeness, condensation, nucleon superfluidity, and cooling of neutron stars, Astrophys. J. Lett. **354**, L17 (1990).
[27] M. Prakash, M. Prakash, J. M. Lattimer, and C. J. Pethick, Rapid cooling of neutron stars by hyperons and Delta isobars, Astrophys. J. Lett. **390**, L77 (1992).
[28] D. Page, U. Geppert, and F. Weber, The cooling of compact stars, Nucl. Phys. A **777**, 497 (2006).
[29] R. Negreiros, L. Tolos, M. Centelles, A. Ramos, and V. Dexheimer, Cooling of small and massive hyperonic stars, Astrophys. J. **863**, 104 (2018).
[30] T. Fischer, N.-U. F. Bastian, M.-R. Wu, P. Baklanov, E. Sorokina, S. Blinnikov, S. Typel, T. Klähn, and D. B. Blaschke, Quark deconfinement as a supernova explosion engine for massive blue supergiant stars, Nat. Astron. **2**, 980 (2018).
[31] H. Grigorian, D. N. Voskresensky, and K. A. Maslov, Cooling of neutron stars in "nuclear medium cooling scenario" with stiff equation of state including hyperons, Nucl. Phys. A **980**, 105 (2018).
[32] A. R. Raduta, A. Sedrakian, and F. Weber, Cooling of hypernuclear compact stars, Mon. Not. R. Astron. Soc. **475**, 4347 (2018).
[33] A. R. Raduta, J. J. Li, A. Sedrakian, and F. Weber, Cooling of hypernuclear compact stars: Hartree-Fock models and high-density pairing, Mon. Not. R. Astron. Soc. **487**, 2639 (2019).
[34] A. Y. Potekhin, D. A. Zyuzin, D. G. Yakovlev, M. V. Beznogov, and Y. A. Shibanov, Thermal luminosities of cooling neutron stars, Mon. Not. R. Astron. Soc. **496**, 5052 (2020).
[35] M. Fortin, A. R. Raduta, S. Avancini, and C. Providência, Thermal evolution of relativistic hyperonic compact stars with calibrated equations of state, Phys. Rev. D **103**, 083004 (2021).
[36] F. Anzuini, A. Melatos, C. Dehman, D. Viganò, and J. A. Pons, Fast cooling and internal heating in hyperon stars, Mon. Not. R. Astron. Soc. **509**, 2609 (2022).
[37] T. Salmi, D. Choudhury, Y. Kini, T. E. Riley, S. Vinciguerra, A. L. Watts, M. T. Wolff, Z. Arzoumanian, S. Bogdanov, D. Chakrabarty, K. Gendreau, S. Guillot, W. C. G. Ho, D. Huppenkothen, R. M. Ludlam, S. M. Morsink, and P. S. Ray, The radius of the high-mass pulsar PSR J0740+6620 with 3.6 yr of NICER data, Astrophys. J. **974**, 294 (2024).
[38] S. Vinciguerra, T. Salmi, A. L. Watts, D. Choudhury, T. E. Riley, P. S. Ray, S. Bogdanov, Y. Kini, S. Guillot, D. Chakrabarty, W. C. G. Ho, D. Huppenkothen, S. M. Morsink, Z. Wadiasingh, and M. T. Wolff, An updated mass-radius analysis of the 2017–2018 NICER data set of PSR J0030+0451, Astrophys. J. **961**, 62 (2024).
[39] A. J. Dittmann, M. C. Miller, F. K. Lamb, I. M. Holt, C. Chirenti, M. T. Wolff, S. Bogdanov, S. Guillot, W. C. G. Ho, S. M. Morsink, Z. Arzoumanian, and K. C. Gendreau, A more precise measurement of the radius of PSR J0740+6620 using updated NICER data, Astrophys. J. **974**, 295 (2024).
[40] N. Rutherford, M. Mendes, I. Svensson, A. Schwenk, A. L. Watts, K. Hebeler, J. Keller, C. Prescod-Weinstein, D. Choudhury, G. Raaijmakers, T. Salmi, P. Timmerman, S. Vinciguerra, S. Guillot, and J. M. Lattimer, Constraining the dense matter equation of state with new NICER mass–radius measurements and new chiral effective field theory inputs, Astrophys. J. Lett. **971**, L19 (2024).
[41] B. P. Abbott, *et al.*, GW170817: Observation of gravitational waves from a binary neutron star inspiral, Phys. Rev. Lett. **119**, 161101 (2017).
[42] B. P. Abbott, *et al.*, GW170817: Measurements of neutron star radii and equation of state, Phys. Rev. Lett. **121**, 161101 (2018).
[43] B. P. Abbott, *et al.*, Properties of the binary neutron star merger GW170817, Phys. Rev. X **9**, 011001 (2019).
[44] B. P. Abbott, *et al.*, GW190425: Observation of a compact binary coalescence with total mass $\sim$3.4 $M_\odot$, Astrophys. J. Lett. **892**, L3 (2020).
[45] B. P. Abbott, *et al.*, Exploring the sensitivity of next generation gravitational wave detectors, Class. Quantum Grav. **34**, 044001 (2017).
[46] P. S. Ray, *et al.*, STROBE-X mission overview, arXiv:2410.08342.
[47] A. Abac, *et al.*, The science of the Einstein telescope, arXiv:2503.12263.
[48] A. Li, *et al.*, Dense matter in neutron stars with eXTP, Sci. China Phys. Mech. Astron. **68**, 119503 (2025).
[49] D. Lonardoni, A. Lovato, S. Gandolfi, and F. Pederiva, Hyperon puzzle: Hints from quantum Monte Carlo calculations, Phys. Rev. Lett. **114**, 092301 (2015).
[50] I. Vidaña, V. M. Sarti, J. Haidenbauer, D. L. Mihaylov, and L. Fabbietti, Neutron star properties and femtoscopic constraints, Eur. Phys. J. A **61**, 59 (2025).
[51] J. L. Zdunik, P. Haensel, and R. Schaeffer, Phase transitions in stellar cores. II—Equilibrium configurations in general relativity, Astron. Astrophys. **172**, 95 (1987).
[52] S. Blacker, H. Kochankovski, A. Bauswein, A. Ramos, and L. Tolos, Thermal behavior as indicator for hyperons in binary neutron star merger remnants, Phys. Rev. D **109**, 043015 (2024).
[53] H. Kochankovski, G. Lioutas, S. Blacker, A. Bauswein, A. Ramos, and L. Tolos, The impact of hyperons on neutron star mergers: Gravitational waves, mass ejection and black hole formation, Phys. Rev. D **112**, 023014 (2025).
[54] N. K. Glendenning, Neutron stars are giant hypernuclei? Astrophys. J. **293**, 470 (1985).
[55] H. Müther, M. Prakash, and T. Ainsworth, The nuclear symmetry energy in relativistic Brueckner-Hartree-Fock calculations, Phys. Lett. B **199**, 469 (1987).
[56] R. B. Wiringa, V. Fiks, and A. Fabrocini, Equation of state for dense nucleon matter, Phys. Rev. C **38**, 1010 (1988).
[57] S. Goriely, N. Chamel, and J. M. Pearson, Further explorations of Skyrme-Hartree-Fock-Bogoliubov mass formulas. XII: Stiffness and stability of neutron-star matter, Phys. Rev. C **82**, 035804 (2010).
[58] J. M. Lattimer and D. F. Swesty, A generalized equation of state for hot, dense matter, Nucl. Phys. A **535**, 331 (1991).

[59] Y. Sugahara and H. Toki, Relativistic mean-field theory for unstable nuclei with non-linear σ and ω terms, Nucl. Phys. A **579**, 557 (1994).

[60] H. Toki, D. Hirata, Y. Sugahara, K. Sumiyoshi, and I. Tanihata, Relativistic many body approach for unstable nuclei and supernova, Nucl. Phys. A **588**, c357 (1995).

[61] L. Engvik, E. Osnes, M. Hjorth-Jensen, G. Bao, and E. Ostgaard, Asymmetric nuclear matter and neutron star properties, Astrophys. J. **469**, 794 (1996).

[62] E. Chabanat, P. Bonche, P. Haensel, J. Meyer, and R. Schaeffer, A Skyrme parametrization from subnuclear to neutron star densities Part II. Nuclei far from stabilities, Nucl. Phys. A **635**, 231 (1998).

[63] A. Akmal, V. R. Pandharipande, and D. G. Ravenhall, Equation of state of nucleon matter and neutron star structure, Phys. Rev. C **58**, 1804 (1998).

[64] M. Alford, M. Braby, M. Paris, and S. Reddy, Hybrid stars that masquerade as neutron stars, Astrophys. J. **629**, 969 (2005).

[65] S. Typel, Relativistic model for nuclear matter and atomic nuclei with momentum-dependent self-energies, Phys. Rev. C **71**, 064301 (2005).

[66] B. D. Lackey, M. Nayyar, and B. J. Owen, Observational constraints on hyperons in neutron stars, Phys. Rev. D **73**, 024021 (2006).

[67] J. S. Read, B. D. Lackey, B. J. Owen, and J. L. Friedman, Constraints on a phenomenologically parametrized neutron-star equation of state, Phys. Rev. D **79**, 124032 (2009).

[68] M. Hempel and J. Schaffner-Bielich, A statistical model for a complete supernova equation of state, Nucl. Phys. A **837**, 210 (2010).

[69] S. Typel, G. Röpke, T. Klähn, D. Blaschke, and H. H. Wolter, Composition and thermodynamics of nuclear matter with light clusters, Phys. Rev. C **81**, 015803 (2010).

[70] M. Hempel, T. Fischer, J. Schaffner-Bielich, and M. Liebendörfer, New equations of state in simulations of core-collapse supernovae, Astrophys. J. **748**, 70 (2012).

[71] G. Shen, C. J. Horowitz, and S. Teige, New equation of state for astrophysical simulations, Phys. Rev. C **83**, 035802 (2011).

[72] A. W. Steiner, M. Hempel, and T. Fischer, Core-collapse supernova equations of state based on neutron star observations, Astrophys. J. **774**, 17 (2013).

[73] S. Banik, M. Hempel, and D. Bandyopadhyay, New hyperon equations of state for supernovae and neutron stars in density-dependent hadron field theory, Astrophys. J. Suppl. Series **214**, 22 (2014).

[74] D. Alvarez-Castillo, A. Ayriyan, S. Benic, D. Blaschke, H. Grigorian, and S. Typel, New class of hybrid EoS and Bayesian M-R data analysis, Eur. Phys. J. A **52**, 69 (2016).

[75] V. Dexheimer, Tabulated neutron star equations of state modelled within the chiral mean field model, Publ. Astron. Soc. Aust. **34**, e066 (2017).

[76] L. Tolos, M. Centelles, and A. Ramos, The equation of state for the nucleonic and hyperonic core of neutron stars, Publ. Astron. Soc. Aust. **34**, e065 (2017).

[77] H. Togashi, K. Nakazato, Y. Takehara, S. Yamamuro, H. Suzuki, and M. Takano, Nuclear equation of state for core-collapse supernova simulations with realistic nuclear forces, Nucl. Phys. A **961**, 78 (2017).

[78] S. Furusawa, H. Togashi, H. Nagakura, K. Sumiyoshi, S. Yamada, H. Suzuki, and M. Takano, A new equation of state for core-collapse supernovae based on realistic nuclear forces and including a full nuclear ensemble, J. Phys. G: Nucl. Part. Phys. **44**, 094001 (2017).

[79] A. S. Schneider, L. F. Roberts, and C. D. Ott, Open-source nuclear equation of state framework based on the liquid-drop model with Skyrme interaction, Phys. Rev. C **96**, 065802 (2017).

[80] M. Marques, M. Oertel, M. Hempel, and J. Novak, New temperature dependent hyperonic equation of state: Application to rotating neutron star models and I-Q relations, Phys. Rev. C **96**, 045806 (2017).

[81] M. Fortin, M. Oertel, and C. Providência, Hyperons in hot dense matter: What do the constraints tell us for equation of state? Publ. Astron. Soc. Aust. **35**, e044 (2018).

[82] I. Bombaci and D. Logoteta, Equation of state of dense nuclear matter and neutron star structure from nuclear chiral interactions, Astron. Astrophys. **609**, A128 (2018).

[83] A. S. Schneider, C. Constantinou, B. Muccioli, and M. Prakash, Akmal-Pandharipande-Ravenhall equation of state for simulations of supernovae, neutron stars, and binary mergers, Phys. Rev. C **100**, 025803 (2019).

[84] D. Logoteta, A. Perego, and I. Bombaci, Microscopic equation of state of hot nuclear matter for numerical relativity simulations, Astron. Astrophys. **646**, A55 (2021).

[85] J. R. Stone, V. Dexheimer, P. A. M. Guichon, A. W. Thomas, and S. Typel, Equation of state of hot dense hyperonic matter in the Quark-Meson-Coupling (QMC-A) model, Mon. Not. R. Astron. Soc. **502**, 3476 (2021).

[86] A. Sedrakian and A. Harutyunyan, Delta-resonances and hyperons in proto-neutron stars and merger remnants, Eur. Phys. J. A **58**, 137 (2022).

[87] X. Du, A. W. Steiner, and J. W. Holt, Hot and dense matter equation of state probability distributions for astrophysical simulations, Phys. Rev. C **105**, 035803 (2022).

[88] H. Kochankovski, A. Ramos, and L. Tolos, Equation of state for hot hyperonic neutron star matter, Mon. Not. R. Astron. Soc. **517**, 507 (2022).

[89] H. Kochankovski, A. Ramos, and L. Tolos, Hyperonic uncertainties in neutron stars, mergers, and supernovae, Mon. Not. R. Astron. Soc. **528**, 2629 (2024).

[90] S. Tsiopelas, A. Sedrakian, and M. Oertel, Finite-temperature equations of state of compact stars with hyperons: Three-dimensional tables, Eur. Phys. J. A **60**, 127 (2024).

[91] H. Tong, S. Elhatisari, U.-G. Meißner, and Z. Ren, Multi-strangeness matter from *ab initio* calculations, arXiv:2509.26148.

[92] G. Baym, C. Pethick, and P. Sutherland, The ground state of matter at high densities: Equation of state and stellar models, Astrophys. J. **170**, 299 (1971).

[93] P. Deshmukh and S. Krishnaswamy, Erratum, Pramana **6**, 258 (1976).

[94] J. Friedrich and P.-G. Reinhard, Skyrme-force parametrization: Least-squares fit to nuclear ground-state properties, Phys. Rev. C **33**, 335 (1986).

[95] S.-J. Lee, J. Fink, A. B. Balantekin, M. R. Strayer, A. S. Umar, P. G. Reinhard, J. A. Maruhn, and W. Greiner, Lee et al. reply, Phys. Rev. Lett. **60**, 163 (1988).

[96] M. J. Rhoades-Brown, C. Bottcher, and M. R. Strayer, Feynman–Monte Carlo calculations of electron capture at relativistic collider energies, Phys. Rev. A **40**, 2831 (1989).
[97] N. Glendenning and S. Moszkowski, Reconciliation of neutron-star masses and binding of the Λ in hypernuclei, Phys. Rev. Lett. **67**, 2414 (1991).
[98] P.-G. Reinhard and H. Flocard, Nuclear effective forces and isotope shifts, Nucl. Phys. A **584**, 467 (1995).
[99] G. A. Lalazissis, J. König, and P. Ring, New parametrization for the Lagrangian density of relativistic mean field theory, Phys. Rev. C **55**, 540 (1997).
[100] S. Typel and H. Wolter, Relativistic mean field calculations with density-dependent meson-nucleon coupling, Nucl. Phys. A **656**, 331 (1999).
[101] I. Bombaci, M. Baldo, and G. Burgio, A microscopic study of neutron stars' structure, Int. Astron. Union Colloq. **177**, 657 (2000).
[102] F. Douchin and P. Haensel, A unified equation of state of dense matter and neutron star structure, Astron. Astrophys. **380**, 151 (2001).
[103] A. H. Raduta, A. R. Raduta, P. Chomaz, and F. Gulminelli, Critical behavior in a microcanonical multifragmentation model, Phys. Rev. C **65**, 034606 (2002).
[104] B. K. Agrawal, S. Shlomo, and V. Kim Au, Nuclear matter incompressibility coefficient in relativistic and nonrelativistic microscopic models, Phys. Rev. C **68**, 031304 (2003).
[105] T. Gaitanos, M. Di Toro, S. Typel, V. Baran, C. Fuchs, V. Greco, and H. Wolter, On the Lorentz structure of the symmetry energy, Nucl. Phys. A **732**, 24 (2004).
[106] W. Long, J. Meng, N. V. Giai, and S.-G. Zhou, New effective interactions in relativistic mean field theory with nonlinear terms and density-dependent meson-nucleon coupling, Phys. Rev. C **69**, 034319 (2004).
[107] G. A. Lalazissis, T. Nikšić, D. Vretenar, and P. Ring, New relativistic mean-field interaction with density-dependent meson-nucleon couplings, Phys. Rev. C **71**, 024312 (2005).
[108] T. Maruyama, T. Tatsumi, D. N. Voskresensky, T. Tanigawa, and S. Chiba, Nuclear "pasta" structures and the charge screening effect, Phys. Rev. C **72**, 015802 (2005).
[109] E. N. E. van Dalen, C. Fuchs, and A. Faessler, Effective nucleon masses in symmetric and asymmetric nuclear matter, Phys. Rev. Lett. **95**, 022302 (2005).
[110] B. K. Agrawal, S. Shlomo, and V. K. Au, Determination of the parameters of a Skyrme type effective interaction using the simulated annealing approach, Phys. Rev. C **72**, 014310 (2005).
[111] P. Danielewicz and J. Lee, Symmetry energy I: Semi-infinite matter, Nucl. Phys. A **818**, 36 (2009).
[112] V. Dexheimer and S. Schramm, Proto–neutron and neutron stars in a chiral SU(3) model, Astrophys. J. **683**, 943 (2008).
[113] V. A. Dexheimer and S. Schramm, Novel approach to modeling hybrid stars, Phys. Rev. C **81**, 045201 (2010).
[114] T. Schürhoff, S. Schramm, and V. Dexheimer, Neutron stars with small radii—The role of Δ resonances, Astrophys. J. **724**, L74 (2010).
[115] F. Gulminelli, A. R. Raduta, and M. Oertel, Phase transition toward strange matter, Phys. Rev. C **86**, 025805 (2012).
[116] S. Goriely, N. Chamel, and J. M. Pearson, Further explorations of Skyrme-Hartree-Fock-Bogoliubov mass formulas. XIII. The 2012 atomic mass evaluation and the symmetry coefficient, Phys. Rev. C **88**, 024308 (2013).
[117] Y. Xu, S. Goriely, A. Jorissen, G. L. Chen, and M. Arnould, Databases and tools for nuclear astrophysics applications: Brussels nuclear library (BruSlib), Nuclear Astrophysics Compilation of Reactions II (NACRE II) and nuclear network generator (NetGen), Astron. Astrophys. **549**, A106 (2013).
[118] F. Grill, H. Pais, C. Providência, I. Vidaña, and S. S. Avancini, Equation of state and thickness of the inner crust of neutron stars, Phys. Rev. C **90**, 045803 (2014).
[119] M. Oertel, C. Providência, F. Gulminelli, and A. R. Raduta, Hyperons in neutron star matter within relativistic mean-field models, J. Phys. G: Nucl. Part. Phys. **42**, 075202 (2015).
[120] V. Dexheimer, R. Negreiros, and S. Schramm, Reconciling nuclear and astrophysical constraints, Phys. Rev. C **92**, 012801 (2015).
[121] F. Gulminelli and A. R. Raduta, Unified treatment of subsaturation stellar matter at zero and finite temperature, Phys. Rev. C **92**, 055803 (2015).
[122] R. Blumenfeld, S. Amitai, J. F. Jordan, and R. Hihinashvili, Blumenfeld *et al.* reply, Phys. Rev. Lett. **119**, 039802 (2017).
[123] M. Wang, G. Audi, F. G. Kondev, W. Huang, S. Naimi, and X. Xu, The AME2016 atomic mass evaluation (II). Tables, graphs and references, Chin. Phys. C **41**, 030003 (2017).
[124] H. Pais and S. Typel, Comparison of equation of state models with different cluster dissolution mechanisms, *Nuclear Particle Correlations and Cluster Physics* (World Scientific, Singapore, 2017), pp. 95–132.
[125] C. Gonzalez-Boquera, M. Centelles, X. Viñas, and L. Robledo, New Gogny interaction suitable for astrophysical applications, Phys. Lett. B **779**, 195 (2018).
[126] J. M. Pearson, N. Chamel, A. Y. Potekhin, A. F. Fantina, C. Ducoin, A. K. Dutta, and S. Goriely, Unified equations of state for cold non-accreting neutron stars with Brussels-Montreal functionals. I. Role of symmetry energy, Mon. Not. R. Astron. Soc. **481**, 2994 (2018).
[127] S. Typel, Equations of state for astrophysical simulations from generalized relativistic density functionals, J. Phys. G: Nucl. Part. Phys. **45**, 114001 (2018).
[128] V. Dexheimer, R. D. O. Gomes, S. Schramm, and H. Pais, What do we learn about vector interactions from GW170817? J. Phys. G: Nucl. Part. Phys. **46**, 034002 (2019).
[129] L. Perot, N. Chamel, and A. Sourie, Role of the symmetry energy and the neutron-matter stiffness on the tidal deformability of a neutron star with unified equations of state, Phys. Rev. C **100**, 035801 (2019).
[130] J. M. Pearson, N. Chamel, and A. Y. Potekhin, Unified equations of state for cold nonaccreting neutron stars with Brussels-Montreal functionals. II. Pasta phases in semiclassical approximation, Phys. Rev. C **101**, 015802 (2020).
[131] A. R. Raduta, M. Oertel, and A. Sedrakian, Proto-neutron stars with heavy baryons and universal relations, Mon. Not. R. Astron. Soc. **499**, 914 (2020).
[132] C. Mondal, X. Vinas, M. Centelles, and J. N. De, Structure and composition of the inner crust of neutron stars from Gogny interactions, Phys. Rev. C **102**, 015802 (2020).
[133] B. Wei, Q. Zhao, Z.-H. Wang, J. Geng, B.-Y. Sun, Y.-F. Niu, and W.-H. Long, Novel relativistic mean field Lagrangian guided by pseudo-spin symmetry restoration, Chin. Phys. C **44**, 074107 (2020).

[134] A. Taninah, S. Agbemava, A. Afanasjev, and P. Ring, Parametric correlations in energy density functionals, Phys. Lett. B **800**, 135065 (2020).

[135] V. Allard and N. Chamel, $^1S_0$ pairing gaps, chemical potentials and entrainment matrix in superfluid neutron-star cores for the Brussels-Montreal functionals, Universe **7**, 470 (2021).

[136] V. Dexheimer, R. O. Gomes, T. Klähn, S. Han, and M. Salinas, GW190814 as a massive rapidly rotating neutron star with exotic degrees of freedom, Phys. Rev. C **103**, 025808 (2021).

[137] X. Vinas, C. Gonzalez-Boquera, M. Centelles, C. Mondal, and L. M. Robledo, Unified equation of state for neutron stars based on the Gogny interaction, Symmetry **13**, 1613 (2021).

[138] N. Hornick, L. Tolos, A. Zacchi, J.-E. Christian, and J. Schaffner-Bielich, Erratum: Relativistic parameterizations of neutron matter and implications for neutron stars [Phys. Rev. C **98**, 065804 (2018)], Phys. Rev. C **103**, 039902(E) (2021).

[139] C.-J. Xia, B. Y. Sun, T. Maruyama, W.-H. Long, and A. Li, Unified nuclear matter equations of state constrained by the in-medium balance in density-dependent covariant density functionals, Phys. Rev. C **105**, 045803 (2022).

[140] G. Grams, J. Margueron, R. Somasundaram, and S. Reddy, Confronting a set of Skyrme and χ_{EFT} predictions for the crust of neutron stars: On the origin of uncertainties in model predictions, Eur. Phys. J. A **58**, 56 (2022).

[141] A. Clevinger, J. Corkish, K. Aryal, and V. Dexheimer, Hybrid equations of state for neutron stars with hyperons and deltas, Eur. Phys. J. A **58**, 96 (2022).

[142] J. M. Pearson and N. Chamel, Unified equations of state for cold nonaccreting neutron stars with Brussels-Montreal functionals. III. Inclusion of microscopic corrections to pasta phases, Phys. Rev. C **105**, 015803 (2022).

[143] B. K. Pradhan, D. Chatterjee, R. Gandhi, and J. Schaffner-Bielich, Role of vector self-interaction in neutron star properties, Nucl. Phys. A **1030**, 122578 (2023).

[144] L. Scurto, H. Pais, and F. Gulminelli, Strong magnetic fields and pasta phases reexamined, Phys. Rev. C **107**, 045806 (2023).

[145] P. Char, C. Mondal, F. Gulminelli, and M. Oertel, Generalized description of neutron star matter with a nucleonic relativistic density functional, Phys. Rev. D **108**, 103045 (2023).

[146] M. G. Alford, L. Brodie, A. Haber, and I. Tews, Tabulated equations of state from models informed by chiral effective field theory, Phys. Scr. **98**, 125302 (2023).

[147] M. G. Alford, L. Brodie, A. Haber, and I. Tews, Relativistic mean-field theories for neutron-star physics based on chiral effective field theory, Phys. Rev. C **106**, 055804 (2022).

[148] T. Carreau, F. Gulminelli, and J. Margueron, Bayesian analysis of the crust-core transition with a compressible liquid-drop model, Eur. Phys. J. A **55**, 188 (2019).

[149] C. Providência, M. Fortin, H. Pais, and A. Rabhi, Hyperonic stars and the symmetry energy, Front. Astron. Space Sci. **6**, 13 (2019).

[150] W.-C. Chen and J. Piekarewicz, Building relativistic mean field models for finite nuclei and neutron stars, Phys. Rev. C **90**, 044305 (2014).

[151] H. Pais and C. Providência, Vlasov formalism for extended relativistic mean field models: The crust-core transition and the stellar matter equation of state, Phys. Rev. C **94**, 015808 (2016).

[152] H. Shen, F. Ji, J. Hu, and K. Sumiyoshi, Effects of symmetry energy on equation of state for simulations of core-collapse supernovae and neutron-star mergers, Astrophys. J. **891**, 148 (2020).

[153] L. Scurto, H. Pais, and F. Gulminelli, General predictions of neutron star properties using unified relativistic mean-field equations of state, Phys. Rev. D **109**, 103015 (2024).

[154] P. Char and C. Mondal, Exploring the limits of nucleonic metamodeling using different relativistic density functionals, Phys. Rev. D **111**, 103024 (2025).

[155] P. Char, C. Mondal, T. Alezraa, F. Gulminelli, and M. Oertel, Properties of neutron stars with hyperons within a relativistic metamodel, arXiv:2510.00997.

[156] P. J. Davis, H. D. Thi, A. F. Fantina, F. Gulminelli, M. Oertel, and L. Suleiman, Inference of neutron-star properties with unified crust-core equations of state for parameter estimation, Astron. Astrophys. **687**, A44 (2024).

[157] P. Demorest, T. Pennucci, S. Ransom, M. Roberts, and J. Hessels, Shapiro delay measurement of a two solar mass neutron star, Nature (London) **467**, 1081 (2010).

[158] J. Antoniadis, *et al.*, A massive pulsar in a compact relativistic binary, Science **340**, 1233232 (2013).

[159] R. W. Romani, D. Kandel, A. V. Filippenko, T. G. Brink, and W. Zheng, PSR J0952–0607: The fastest and heaviest known galactic neutron star, Astrophys. J. Lett. **934**, L17 (2022).

[160] H. T. Cromartie, *et al.*, Relativistic Shapiro delay measurements of an extremely massive millisecond pulsar, Nat. Astron. **4**, 72 (2019).

[161] E. Fonseca *et al.*, The NANOGrav nine-year data set: Mass and geometric measurements of binary millisecond pulsars, Astrophys. J. **832**, 167 (2016).

[162] Using $R(M)$ instead of $M(R)$ avoids infinite derivatives on the stable branch of the mass-radius relation except for the configuration at $M_{\max}$. We employ a second-order accurate finite differencing with variable step size.

[163] K. Chatziioannou, Uncertainty limits on neutron star radius measurements with gravitational waves, Phys. Rev. D **105**, 084021 (2022).

[164] C. Pacilio, A. Maselli, M. Fasano, and P. Pani, Ranking Love numbers for the neutron star equation of state: The need for third-generation detectors, Phys. Rev. Lett. **128**, 101101 (2022).

[165] F. Iacovelli, M. Mancarella, C. Mondal, A. Puecher, T. Dietrich, F. Gulminelli, M. Maggiore, and M. Oertel, Nuclear physics constraints from binary neutron star mergers in the Einstein telescope era, Phys. Rev. D **108**, 122006 (2023).

[166] A. Bandopadhyay, K. Kacanja, R. Somasundaram, A. H. Nitz, and D. A. Brown, Measuring neutron star radius with second and third generation gravitational wave detector networks, Class. Quantum Grav. **41**, 225003 (2024).

[167] D. Finstad, L. V. White, and D. A. Brown, Prospects for a precise equation of state measurement from Advanced LIGO and Cosmic Explorer, Astrophys. J. **955**, 45 (2023).

[168] K. Walker, R. Smith, E. Thrane, and D. J. Reardon, Precision constraints on the neutron star equation of state with third-generation gravitational-wave observatories, Phys. Rev. D **110**, 043013 (2024).

[169] G. Huez, S. Bernuzzi, M. Breschi, and R. Gamba, Kilohertz gravitational waves from binary neutron star mergers: Full

spectrum analyses and high-density constraints on neutron star matter, arXiv:2507.06293.

[170] W.-J. Xie and B.-A. Li, Bayesian inference of the symmetry energy of superdense neutron-rich matter from future radius measurements of massive neutron stars, Astrophys. J. **899**, 4 (2020).

[171] S. Han and M. Prakash, On the minimum radius of very massive neutron stars, Astrophys. J. **899**, 164 (2020).

[172] T. Zhao and J. M. Lattimer, Quarkyonic matter equation of state in beta-equilibrium, Phys. Rev. D **102**, 023021 (2020).

[173] M. Ferreira and C. Providência, Constraining neutron star matter from the slope of the mass-radius curves, Phys. Rev. D **110**, 063018 (2024).

[174] B.-A. Li, X. Grundler, W.-J. Xie, and N.-B. Zhang, Bayesian inference of fine features of the nuclear equation of state from future neutron star radius measurements to 0.1 km accuracy, Phys. Rev. D **110**, 103040 (2024).

[175] B.-J. Cai and B.-A. Li, Novel scalings of neutron star properties from analyzing dimensionless Tolman–Oppenheimer–Volkoff equations, Eur. Phys. J. A **61**, 55 (2025).

[176] S.-P. Tang, Y.-J. Huang, and Y.-Z. Fan, Phase transition and nuclear symmetry energy from neutron star observations: Constraints in light of PSR J0614-3329, Phys. Rev. D **112**, 083009 (2025).

[177] P. J. Kalita, T. Malik, T. Zhao, B. Kumar, and J. M. Lattimer, Observable signatures of a quarkyonic phase in neutron stars, arXiv:2510.23405.

[178] M. Durante, P. Indelicato, B. Jonson, V. Koch, K. Langanke, U.-G. Meißner, E. Nappi, T. Nilsson, T. Stöhlker, E. Widmann, and M. Wiescher, All the fun of the FAIR: Fundamental physics at the facility for antiproton and ion research, Phys. Scr. **94**, 033001 (2019).

[179] *The CBM Physics Book: Compressed Baryonic Matter in Laboratory Experiments*, edited by B. Friman, C. Hohne, J. Knoll, S. Leupold, J. Randrup, R. Rapp, and P. Senger (2011), Vol. 814.

[180] E. R. Most, L. J. Papenfort, V. Dexheimer, M. Hanauske, S. Schramm, H. Stöcker, and L. Rezzolla, Signatures of quark-hadron phase transitions in general-relativistic neutron-star mergers, Phys. Rev. Lett. **122**, 061101 (2019).

[181] A. Bauswein, N.-U. F. Bastian, D. B. Blaschke, K. Chatziioannou, J. A. Clark, T. Fischer, and M. Oertel, Identifying a first-order phase transition in neutron-star mergers through gravitational waves, Phys. Rev. Lett. **122**, 061102 (2019).

[182] The matching between crust and core EoS can affect radii and tidal deformability and in principle the use of unified EoS models is desirable [183–186]. For considering derivatives especially at higher masses such effects are, however, less relevant.

[183] M. Fortin, C. Providência, A. R. Raduta, F. Gulminelli, J. L. Zdunik, P. Haensel, and M. Bejger, Neutron star radii and crusts: Uncertainties and unified equations of state, Phys. Rev. C **94**, 035804 (2016).

[184] L. Perot, N. Chamel, and A. Sourie, Role of the crust in the tidal deformability of a neutron star within a unified treatment of dense matter, Phys. Rev. C **101**, 015806 (2020).

[185] L. Suleiman, M. Fortin, J. L. Zdunik, and P. Haensel, Influence of the crust on the neutron star macrophysical quantities and universal relations, Phys. Rev. C **104**, 015801 (2021).

[186] A. F. Fantina, J. L. Zdunik, N. Chamel, J. M. Pearson, L. Suleiman, and S. Goriely, Accreting neutron stars from the nuclear energy-density functional theory. II. Equation of state and global properties, Astron. Astrophys. **665**, A74 (2022).